J Mol Model (2012) 18:2377–2386
DOI 10.1007/s00894-011-1255-5

ORIGINAL PAPER

Mapping multiple potential ATP binding sites on the matrix side of the bovine ADP/ATP carrier by the combined use of MD simulation and docking

Daniele Di Marino · Francesco Oteri · Blasco Morozzo della Rocca · Ilda D'Annessa · Mattia Falconi

Received: 23 June 2011 / Accepted: 22 September 2011 / Published online: 12 October 2011

Abstract The mitochondrial adenosine diphosphate/adenosine triphosphate (ADP/ATP) carrier—AAC—was crystallized in complex with its specific inhibitor carboxyatractyloside (CATR). The protein consists of a six-transmembrane helix bundle that defines the nucleotide translocation pathway, which is closed towards the matrix side due to sharp kinks in the odd-numbered helices. In this paper, we describe the interaction between the matrix side of the AAC transporter and the ATP^{4-} molecule using carrier structures obtained through classical molecular dynamics simulation (MD) and a protein–ligand docking procedure. Fifteen structures were extracted from a previously published MD trajectory through clustering analysis, and 50 docking runs were carried out for each carrier conformation, for a total of 750 runs ("MD docking"). The results were compared to those from 750 docking runs performed on the X-ray structure ("X docking"). The docking procedure indicated the presence of a single interaction site in the X-ray structure that was conserved in the structures extracted from the MD trajectory. MD docking showed the presence of a second binding site that was not found in the X docking. The interaction strategy between the AAC transporter and the ATP^{4-} molecule was analyzed by investigating the composition and 3D arrangement of the interaction pockets, together with the orientations of the substrate inside them. A relationship between sequence repeats and the ATP^{4-} binding sites in the AAC carrier structure is proposed.

Keyword Mitochondrial ADP/ATP carrier · Molecular dynamics · Cluster analysis · Protein–ligand docking · ATP–carrier interaction · ATP binding sites

Electronic supplementary material The online version of this article (doi:10.1007/s00894-011-1255-5) contains supplementary material, which is available to authorized users.

D. Di Marino
Department of Medicine,
University of Rome Tor Vergata,
Via Montpellier 1,
00100 Rome, Italy

D. Di Marino
Catholic University of Leuven,
Herestraat 69,
3000 Leuven, Belgium

D. Di Marino
Department for Developmental and Molecular Genetics,
VIB11, Herestraat 49,
3000 Leuven, Belgium

F. Oteri · B. Morozzo della Rocca · I. D'Annessa · M. Falconi
Department of Biology,
University of Rome Tor Vergata,
Via Della Ricerca Scientifica,
Rome 00133, Italy

M. Falconi (✉)
CIBB, Center of Biostatistics and Bioinformatics,
Via della Ricerca Scientifica,
00133 Rome, Italy
e-mail: falconi@uniroma2.it

Introduction

The mitochondrial ADP/ATP carrier (AAC) is an important constituent of the inner mitochondrial membrane that imports ADP^{3-} and exports ATP^{4-} toward the cytosol. Several diseases, such as mitochondrial myopathies and ophthalmoplegia, have been associated with dysfunction of the human ADP/ATP carrier [1–6]. AAC is related to the respiratory chain, which creates a proton gradient across the

inner membrane that is utilized to catalyze ATP synthesis, the essential molecule that provides chemical energy in most cellular reactions. Several energy-generating pathways are localized in the matrix of mitochondria (i.e., the citric acid cycle and fatty acid oxidation), as well as other types of pathways (i.e., synthesis and degradation of amino acids). Heat generation is also triggered at the level of the inner mitochondrial membrane by dissipating the proton gradient [7]. All of these processes require the import and export of protons or metabolites. In spite of large differences among these metabolites, a common feature emerges: a variety of them are transported by carriers belonging to the same family, the mitochondrial carrier family (MCF). The MCF is characterized by a specific amino acid motif, PxD/ExxK/RxK/R-(20–30 residues)-D/EGxxxxaK/RG, where "a" represents an aromatic residue, that is repeated three times in the sequence [8, 9]. The triplication of about 100 amino acids including this motif most probably stems from an ancestral gene duplication [8].

Among all MCF carriers, the AAC is the most abundant in the membrane and represents up to 10% of the proteins that compose the inner membrane of bovine heart mitochondria. For these reasons, it was the first to be characterized [10, 11]. The two inhibitors carboxyatractyloside (CATR) and bongkrekic acid (BA), which both act as strong poisons by blocking nucleotide translocation [12, 13], have been extensively used to characterize different conformational states of the carrier. The CATR stabilizes the c state, in which the protein is opened towards the intermembrane space and closed to the matrix side, while the BA stabilizes the opposite conformation, called the m state, which is closed towards the intermembrane space and opened to the matrix side [14].

On account of its abundance in natural sources, the structure of the AAC was also the first to be explored by electron microscopy [15], and is the only one to be resolved by X-ray crystallography so far [16]. The AAC has been crystallized in the presence of the inhibitor CATR [17], which is known to bind to the carrier from the intermembrane space (IMS), hampering ADP^{3-} import. The structure was solved to 2.2 Å resolution [17, 18], revealing for the first time the overall fold of MCF carriers and highlighting the role played by the MCF motif in the folding.

The structure of the ADP/ATP mitochondrial transporter is characterized by a six-transmembrane helix bundle with the chain termini located in the intermembrane space (IMS). The transmembrane helices are linked by two loops located in the IMS and by three matrix domains. Each matrix domain consists of two loops that include one small α-helix (loop–helix–loop domain). The three loops are called M1, M2, and M3, following the sequence order, while the three short α-helices that are enclosed in these loops are called H1-2, H3-4, and H5-6, depending on the long helices connected by each loop [17].

However, transport dynamics and mechanisms remain elusive. It appears that the wobbling of odd-numbered helices and rearrangements of salt-bridge networks are important elements for the transport process [19], which lead to an interchange of cytoplasm and matrix accessibility, as hinted by mass spectrometry data coupled to H-D exchange in the presence of both inhibitors [20].

The structure resolved in the presence of CATR is a good model to use to understand the interactions of the carrier with the ADP^{3-} substrate [17]. This issue has been addressed through MD simulation in two papers, which have shown an electrostatic funneling mechanism [21, 22]. The protein's electrostatic potential attracts the substrate towards the channel, and allows the ADP^{3-} to rapidly enter the helical bundle. The positively charged carrier residues, which electrostatically interact with the phosphate groups, drive the passage of the substrate through the cavity to its bottom [21, 22]. In fact, high chloride concentration conditions cause inhibition of binding and the further transport of nucleotides [23]. Moreover, tyrosine residues facing the cavity are the targets of SRC kinases that modulate transport by phosphorylation [24].

These simulation studies have focused on the IMS side of the carrier [21, 22], while the substrate binding, which occurs from the matrix side, remains elusive. Experimental works have addressed this issue through the use of nucleotide analogs that bind the carrier but are not transported. Some works with reactive analogs have hinted that M2 loop residues are involved with substrate binding on the matrix side [25, 26].

Identifying the binding sites between the ATP molecule and the carrier matrix side may add a further detail to the description of ADP/ATP transport function. At present, the available 3D structure of the carrier, solved in complex with the CATR inhibitor [17], is deemed unsuitable for recognizing ATP ligands from the matrix lumen. However, it has been shown that, even in the presence of CATR, the ADP/ATP carrier can recognize, fluorescein derivatives (such as eosin Y) from the matrix lumen that are structurally related to adenine nucleotides, although it cannot transport them [26]. The binding of eosin Y is displaced by ADP or ATP, which prevents the thiol-reactive eosin-5-maleimide molecule from binding to Cys159, thus suggesting that ATP binds near to this residue, mainly through hydrophobic interactions [25, 26]. Taking this work into account, the available 3D structure of the carrier can then be taken as an initial model to verify its ability to bind the ATP molecule from the matrix lumen. This hypothesis is reinforced by observations made based on a previous carrier MD simulation carried out in the absence of CATR [19], which showed that the matrix region of the protein undergoes

significant changes leading to the appearance of matrix cavities (not found in the crystal) that may provide ATP-binding sites. In a recent paper, MD simulations of the wild-type ADP/ATP carrier and the single Ala113Pro and double Ala113Pro/Val180Met mutants were carried out to shed light on the structural–dynamical changes induced by the Val180Met mutation that restores the carrier function in the Ala113Pro pathologic mutant [27]. In this work, analysis of the correlated and anticorrelated motions indicated that, in particular in the matrix region, the wild-type correlation pattern that is altered in the single mutant is restored by the double mutation [27], indicating that correlations in the motions of the matrix region represent a functional feature of the transporter.

In the work reported in this paper, in order to estimate the ability of the carrier matrix region to recognize the ATP molecule, the structures of a previously generated MD trajectory [19, 27] were clustered, and each representative structure was used to carry out extensive docking runs with the ATP molecule. Docking results were also clustered, and possible binding sites were recognized and mapped. The interacting residues were identified, along with the specific interaction type, and were compared with those identified in the crystal structure, suggesting implications for multiple ATP binding sites related to the AAC tripartite structure.

Methods

MD simulation and clustering of the MD trajectory

The MD simulation of the wild-type bovine ADP/ATP carrier was carried out as described in a previous paper [19, 27]. The last 20 ns of the MD trajectory were clustered through the g_cluster program in the GROMACS 3.3.3 package [28] using the Gromos algorithm [29]. The clustering procedure starts by calculating the relative RMSD between all conformations of the trajectory in order to build an $N(N-1)/2$ matrix of RMSD values, where N is the number of values extracted from the 40,000 saved structures. The program defines the neighbor configurations and the number of neighbors for each configuration. The configuration with the highest number of neighbors is taken as representative of the first cluster, which will present this structure, together with all of its neighbors. The structures of this first cluster are then removed from the pool, and the procedure is iterated. In this way, all of the configurations are assigned to just one cluster. The number of clusters depends on the threshold value adopted and, in this case, to obtain a maximum number of 34 clusters, a threshold value of 1.5 Å was used. The first 15, out of 34, clusters were used for the analysis, since they contain almost all of the sampled conformations (i.e., about 96% of the trajectory structures).

Docking and clustering of the ATP^{4-} molecule

Protein–ligand docking is a simulative method that predicts the preferred orientation of a ligand molecule with respect to a protein receptor by evaluating the strength of their association using energetic and geometric scoring functions. Protein–ligand docking runs were performed using a Lamarckian genetic algorithm [30] through the Autodock 4.0 program [31]. Seven hundred fifty independent runs were performed on the X-ray (PDB code 1OKC) structure, and 50 independent runs were carried out for each of 15 cluster representative configurations identified from the MD trajectory, yielding a total of 750 runs. For the sake of clarity, docking on the X-ray structure will be termed "X docking" here, while docking on the structures extracted from the molecular dynamics trajectory will be termed "MD docking." The center of a 38.3 × 42.0 × 19.5 Å grid was placed over the geometric center of the matrix portion of the carrier (Fig. S1 of the "Electronic supplementary material," ESM). The dimensions and the position of the docking grid chosen cause it to cover the entire region of the protein protruding from the lipid bilayer. The complexes were inspected through an in-house-modified version of the g_mindist program in the GROMACS 3.3.3 package [28]. This analysis was done in order to better characterize the binding sites by selecting the protein atoms within a distance of 3.5 Å from any ATP atom.

Clustering of the ATP-docked structures was carried out using the same procedure described above for MD structure clustering, but using a threshold value of 1.2 Å, which generates five clusters for the X docking and ten clusters for the MD docking. In the case of the X docking, the first cluster includes 98% of the docked complexes. In the case of MD docking, the first two clusters include 85% of the docked complexes.

In order to assess ATP^{4-} binding specificity, 750 docking runs were also carried out for the GTP^{4-} molecule on the X-ray structure and on the same 15 MD structures, each representing a cluster, extracted from the MD simulation.

Multiple sequence alignment

The ADP/ATP transporter sequences were extracted from the SwissProt database. Sequences from putative carriers were excluded, as well as transporter sequences from plants that, due to their evolutionary distance and length variability, impede the correct execution of the multiple alignment algorithm. The multiple alignment of 33 sequences (as shown in the ESM) was performed using the ClustalW program with default settings (http://www.

ebi.ac.uk/clustalw/). When present, isoforms 1 and 2 of the same species were both included.

Graphs and images

Graphs were obtained with the Grace program (http://plasma-gate.weizmann.ac.il/Grace/), and images were obtained with the VMD visualization package [32] and the UCSF Chimera program [33].

Results

Clustering of the MD trajectory

The ensemble of carrier conformations generated from the MD simulation was pruned and grouped into families with similar structures via a clustering analysis performed using the g_cluster [28] tool of the GROMACS package. This procedure was then repeated by iteration until all of the structures were assigned to a cluster. The structures representative of each cluster were selected to carry out the docking with the ATP^{4-} molecule. Choosing a threshold of 1.5 Å, 34 clusters were identified and ordered according to their populations in Fig. 1a. The first 15 clusters, which encompassed more than 95% of the sampled conformations (Fig. 1b), were selected for the docking analysis.

Docking of the ATP^{4-} molecule

In the molecular docking of the ATP^{4-} molecule to the carrier (carried out using the program AutoDock [30, 31]), the complete matrix region of the protein, which protrudes from the phospholipid bilayer, was considered in order to take into account the widest possible area of substrate interaction with the protein (Fig. S1). Seven hundred fifty docking runs were carried out on the X-ray structure of the mitochondrial ADP/ATP transporter, and 50 docking runs were carried out for each of the 15 structures (each of which was representative of one of the 15 clusters), again giving a total of 750 complexes. The final results from the 750 X and MD docking runs are shown in Fig. 2a and b, respectively, where the ATP^{4-} molecule is represented by its center of mass. In the case of X docking (Fig. 2a) a preferential interaction site was identified, whereas for MD docking (Fig. 2b), the centers of mass of the docked ATP^{4-} molecules are more spread out on the protein, and cover approximately half of the matrix-side surface. In MD docking, due to favorable conformations of the positively charged lipids, some ATP molecules can also interact with the membrane surface (Fig. 2b). These interactions were not detected in the case of X docking (Fig. 2a), where the double layer (in a crystalline starting conformation) hampers the interactions between the ATP molecules and the membrane surface due to poor exposure of the phospholipid charges. The docking energies range from −11.4 to −5.8 kcal mol^{-1} for X docking (Fig. 2a), while in MD docking (Fig. 2b), the docking energies range from −11.2 to −5.8 kcal mol^{-1} for site I and from −10.2 to −6.2 kcal mol^{-1} for site II.

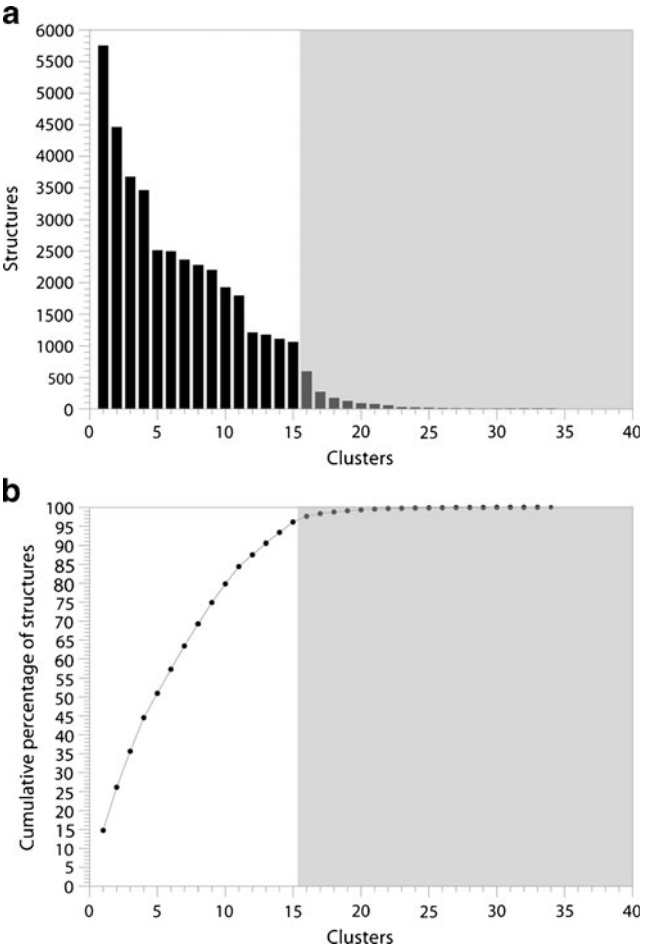

Fig. 1 MD trajectory clustering. **a** Histogram of the clusters extracted from the analysis of the 20 ns MD trajectory. The *gray box* represents the lowest populated clusters, which were not taken into account for the docking analysis. **b** Cumulative percentages of the number of structures belonging to each cluster. The *gray box* shows the cumulative percentages related to the clusters not taken into account in the docking analysis

The structures of the bimolecular carrier–ATP^{4-} complexes resulting from X docking and MD docking were clustered to select the preferred complexes. The results of the clustering in the X docking runs (Fig. 3a, black bars) show the presence of a unique family of ATP^{4-} configurations with a single preferential orientation, as represented by site I in Fig. 3b, where the position of the phosphate moiety of the ATP^{4-} is indicated by a square, that of the sugar by a line, and that of the base by a circle.

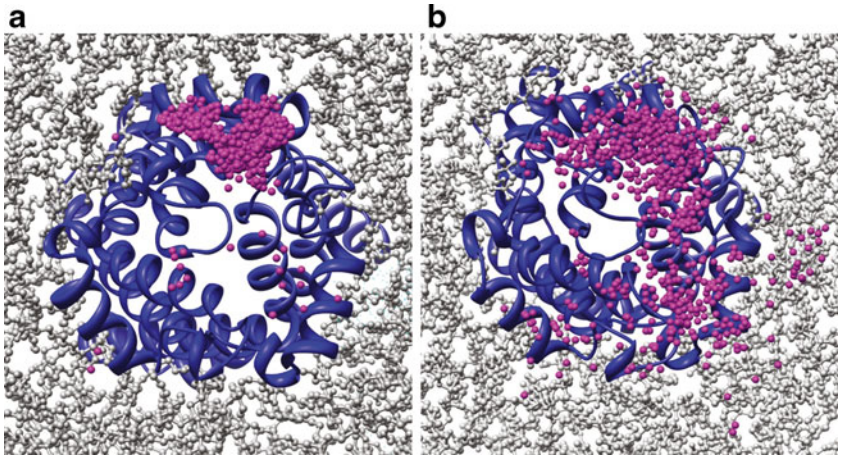

Fig. 2 Docking results. **a**, **b** Ribbon representations of the X-ray and MD average structures of the protein, respectively, colored in *blue* and immersed in a lipid bilayer (represented as *gray balls and sticks*). In both cases, the *pink balls* represent the spread of the centers of mass of 750 ATP^{4-} molecules docked on the X-ray structure (**a**), and of 750 ATP^{4-} molecules docked on the representative structures of the 15 clusters extracted from the MD simulation (**b**). In X docking (**a**), the crystalline state of the lipids means that they cannot form stable interactions with the ATP molecules, while in MD docking (**b**), the double layer explores conformations that allow the interaction of ATP ligands with the membrane surface

In the case of MD docking (Fig. 3a, red bars) several clusters were identified, but two were predominant, and these represented about 85% of the 750 ATP^{4-} docked complexes. The most representative one, including about 400 structures, matched the site observed in the X docking, indicating that it was preserved during the dynamics and is represented by site I in Fig. 3c. The other representative site was detected in about 200 structures and was identified as site II in Fig. 3c.

GTP^{4-} docking was performed to evaluate the specificity of the ATP^{4-} binding sites found in X and MD docking, using the same procedure and structures as for ATP. In both docking simulations, the GTP^{4-} interacts with the carrier through the phosphate groups but not through the base, strongly suggesting that the identified sites are specific for ATP^{4-}. Moreover, in the MD docking, GTP^{4-} is found spread over the entire matrix region, indicating the absence of specific interaction sites (Fig. S2). Indeed, the binding free energies for ATP^{4-} and GTP^{4-} are very different; their average values for the X docking runs were −8.13 (± 0.89) and −2.52 (± 0.81) kcal mol^{-1}, respectively. For MD

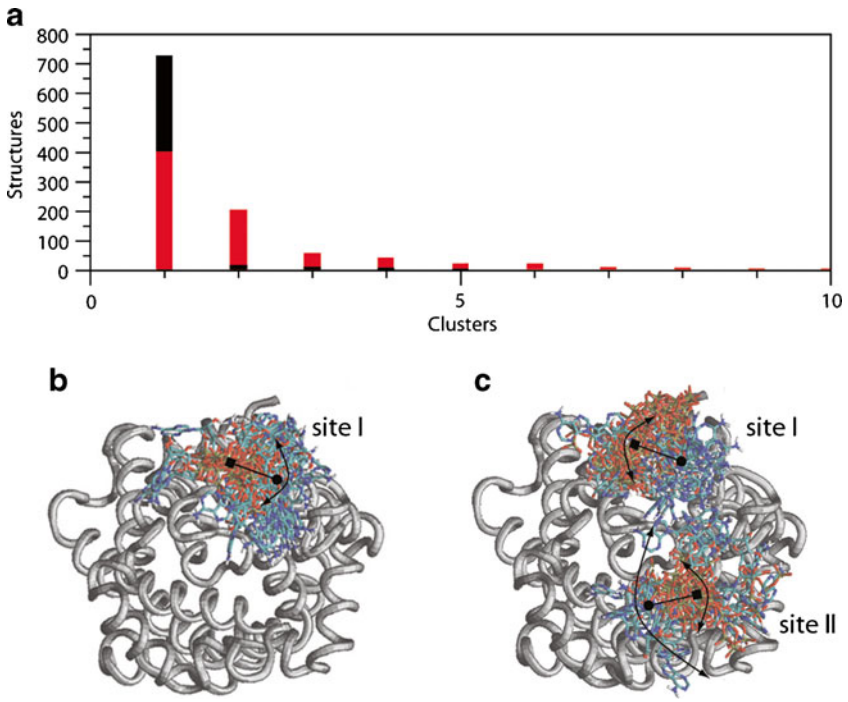

Fig. 3 Docking clustering. **a** Histograms of the clusters of the 750 ATP^{4-} docked molecules on the X-ray structures (*black bars*) and on the 15 representative structures extracted from the 20 ns molecular dynamic simulations (*red bars*). Localization on the protein (*gray ribbon*) of the ATP^{4-} molecule as observed in X docking (**b**) and in MD docking (**c**). ATP^{4-} is represented schematically by a *circle*, a *line*, and a *square* representing the base, the sugar, and the phosphates, respectively. The *width of the arrow* indicates the spread of the position

docking, the average binding free-energy values for ATP^{4-} were: −8.47 (± 0.87) kcal mol^{-1} for site I and −8.22 (± 0.84) kcal mol^{-1} for site II, while the average value for the docked GTP^{4-} molecule was −4.76 (± 1.26) kcal mol^{-1}, confirming the specificity of the binding sites for ATP^{4-}.

Binding site analyses

The contacts between all of the atoms of the ATP^{4-} molecule and those of the protein matrix region were calculated using a modified version of the g_mindist program in the GROMACS 3.3.3 package [28]. Each occasion that the atoms were separated by a distance of less than 3.5 Å in at least 10% of the complexes is reported in Table 1. In the X docking runs, the amino acids involved in the binding of ATP^{4-} are Gln43, Lys48, Arg59, and Glu63, located in the C-terminal region of the M1 loop and on the small helix H1-2, as well as Gly145, Lys146, and Gln150, located on the M2 loop (Figs. 4 and S3 in the ESM). Analysis of the percentages of interaction with the three portions of the substrate (Table 1a) indicates that the positively charged amino acids (Lys48, Arg59, Lys146) are involved in interactions with the negative phosphate groups, while the glutamines (Gln43 and Gln150)

Table 1 Protein–ATP^{4-} contacts: percentages of contact between the carrier amino acids and any atom of the ATP^{4-} molecules observed during X docking (A) and in the MD docking (B)

		Phosphate	Sugar	Base
Site I	A			
	Gln43	1	33	66
	Lys48	63	25	12
	Arg59	59	21	20
	Glu63	70*	13	17
	Gly145	1	40	58
	Lys146	55	27	18
	Gln150	1	32	67
Site I	B			
	Lys48	58	20	22
	Gln49	45	25	30
	Arg59	53	30	17
	Glu63	14	56	30
	Gly145	9	40	51
	Lys146	46	29	25
	Gln150	20	23	58
Site II	Lys42	55	22	23
	Gln240	26	28	46
	Arg243	50	22	28
	Asp247	22	53	25
	Met249	22	35	43

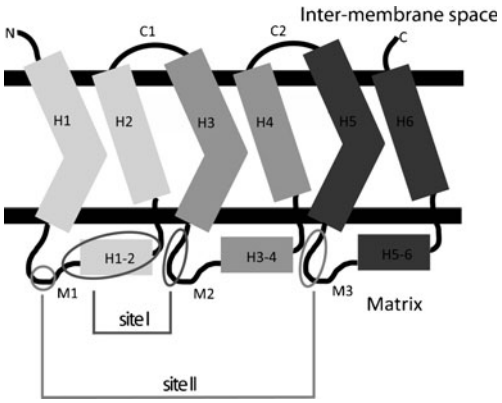

Fig. 4 Protein regions involved in binding. A 2D topology view of the ADP/ATP carrier indicating the positions of the protein regions (sites I and II) involved in the formation of the ATP^{4-} binding sites is shown. The three carrier repeats are highlighted using a different grayscale

are involved with the base moiety. It is interesting to note that Glu63, a negatively charged amino acid, is involved in the formation of the ATP^{4-} recognition site, and is often at a distance of <3.5 Å from the phosphate moiety (Table 1a and Fig. 5a). The interaction between two molecules with the same charge is unfavorable, but Glu63 has an indirect role: a negatively charged residue is required to stabilize the positively charged residues Arg59 and Lys146, forming a salt bridge network and ensuring the correct orientations of the positive residues that interact with the phosphate moiety. The last amino acid to represent an ATP^{4-} interaction site is Gly145, which, due to its lack of a side chain, generates a cavity where the base moiety of the ATP^{4-} molecule can be accommodated.

The amino acids involved in the interaction with the ligand at the first site in MD docking are Lys48, Gln49, Arg59, Glu63, Gly145, Lys146, and Gln150 (Table 1b). They largely overlap with those found at site I in X docking, apart from Gln43; in X docking, Gln43 interacts with the base moiety, but in MD docking it is replaced by Gln49, which interacts with the phosphate (Table 1, movie M1 and Fig. S3B). A further difference is that, in MD docking, Glu63 interacts with the sugar moiety (Table 1b and Fig. 5b).

MD docking identified another interaction site (site II), involving Lys42, Gln240, Arg243, Asp247, Met249, Lys42 located on the M1 loop, and another four amino acids located on the M3 loop (Fig. 4). The amino acid composition of this site was similar to the one observed at site I, consisting of two positive amino acids (Lys42 and Arg243) interacting with the phosphate groups, a glutamine (Gln240) interacting with the base, a negatively charged amino acid (Asp247) interacting with the sugar moiety, and a methionine (Met249) assisting Gln240 in the base interaction (see Table 1b, Figs. 4, 5c and S3 and movie M1).

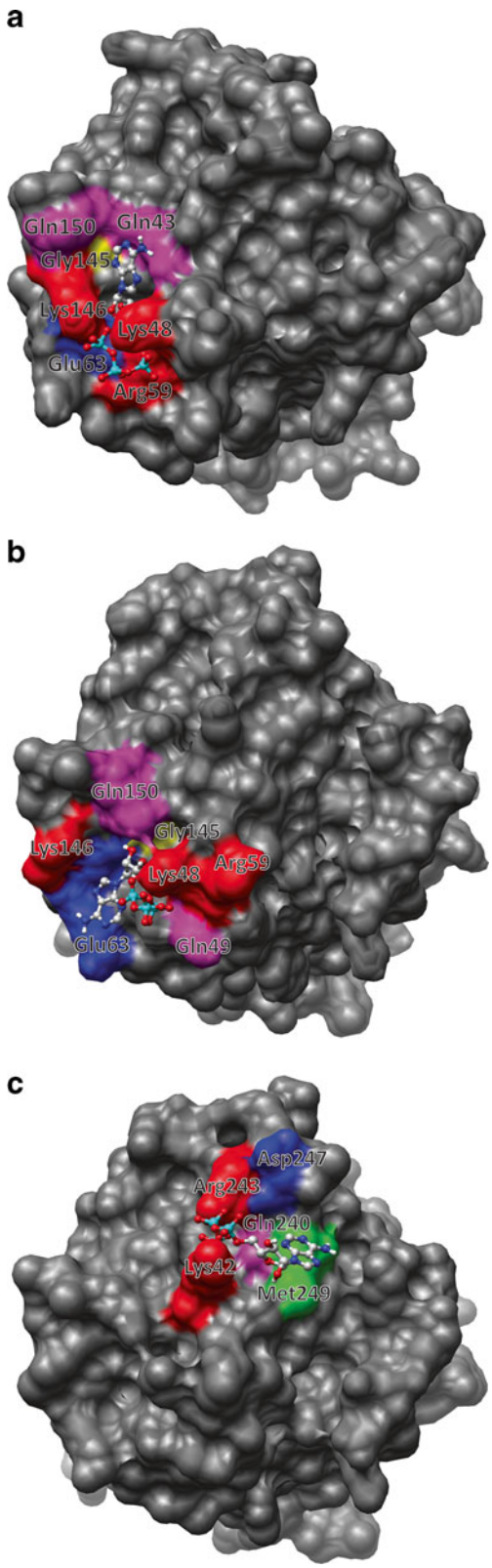

Fig. 5 Residues at binding sites. The figures depict representative carrier–ATP^{4-} complexes showing site I identified in X docking (**a**) and site I (**b**) and site II (**c**) identified in MD docking. *Red and blue spots* indicate positive and negative amino acid charges, respectively. *Magenta, yellow, and green spots* represent Gln, Gly, and Met residues

For the two sites extracted from MD docking, the orientation and the spread of the ligand over the protein were correlated to the mobility of the interacting amino acids. Figure 6 shows the per-residue RMSF (root mean square fluctuations) of the whole protein calculated along the considered MD trajectory, where the residues at the first and second binding sites are marked with dark and light gray bars, respectively. Lys48, Lys146, and Arg59 had fluctuation values that were higher than those of the other interacting amino acids, explaining the large spread of the phosphate groups observed at site I in Fig. 3d. Similarly, the low spread observed for the base and sugar moieties can be explained by the low fluctuations of the amino acids interacting with them (Glu63, Gln150) (Fig. 6). In the case of site II, the spread of the phosphates was intermediate, since Arg243 had a high fluctuation value whilst Lys42 had a low fluctuation value (Figs. 3d, 6). The spreads were higher for the base and sugar, which are contacted by amino acids (Gln240, Asp247, and Met249) characterized by large fluctuation values (Fig. 6). It is interesting to note that there was also a spread in base position in the rigid X docking, which can be explained by the presence of two glutamine residues that can equally interact with the adenine ring (Fig. 5a and Table 1a).

Discussion

Although the X-ray structure provides important details, it gives a static snapshot of biological function, thus limiting attempts to understand the transport mechanism. The crystal structure blocked by the inhibitor in the c state represents the conformation that is closed towards the mitochondrial matrix and opened towards the intermembrane space [34]. Previously, the existence of three contact points was demonstrated for various substrates, including ATP^{4-}, which is conserved in all mitochondrial transporters and located in the transmembrane bundle [35]. Further analysis, performed through symmetric sequence analysis, confirmed these findings and also detected two conserved areas for the ligand interaction: the bottom of the channel and towards the side of the intermembrane space [36]. These aspects were also confirmed by molecular dynamics simulations [20, 21].

In the present work, our attention has been focused on the matrix carrier region located outside the membrane. The analysis, which was carried out on both the X-ray structure and representative structures extracted from the MD simulation [27], allowed us to understand how the structural sampling of the MD simulation in the absence of CATR is related to the retention or formation of binding sites for the ATP^{4-} substrate. Seven hundred fifty docking runs carried out on the crystal structure clearly showed the

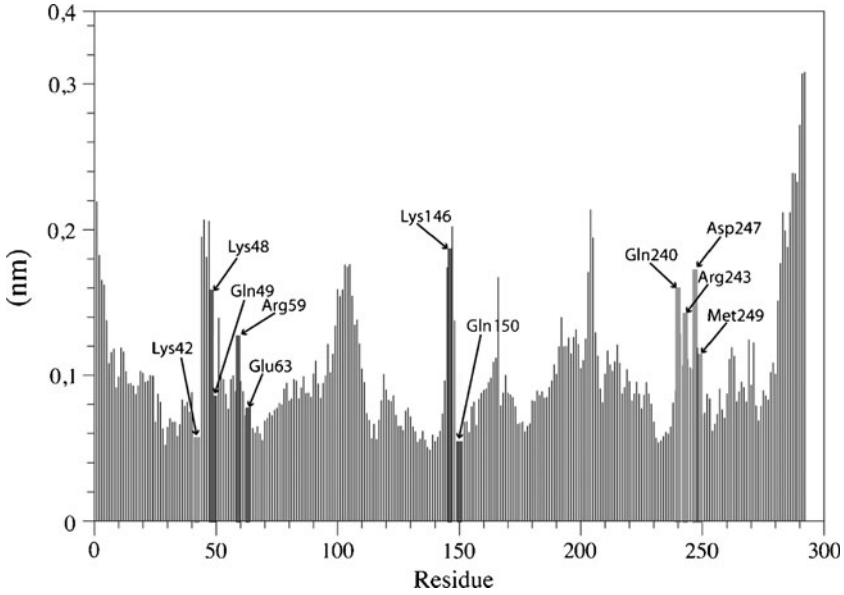

Fig. 6 Protein RMSF. Average per-residue root mean square fluctuations of the ADP/ATP carrier. The *dark and light gray bars* indicate the fluctuations of the residues belonging to sites I and II, respectively. The *black thin bars* show the fluctuations of the residues that are not involved in ATP recognition

presence of a unique ATP^{4-} binding site located on the H1-2 helix and on the M2 loop, in line with the experimental results, identifying hydrophobic residues flanking Cys159 as putative partners for the interaction with the substrate [26]. This result indicates that the region protruding within the mitochondrial matrix has a preformed interaction site, although the protein is in a conformation arranged for transport from the cytoplasmic side. As a matter of fact, it has been reported that the carrier can bind nucleotide analogs on the matrix side, even in the presence of CATR [26]. Moreover, kinetic experiments show that the protein can form an ADP-carrier–ATP ternary complex during transport [37], suggesting that ATP from the matrix side may still bind CATR-bound AAC, although it cannot be transported because the carrier is fixed in an abortive c′ state [14]. The interaction site identified here could function as a regulator of protein activity, as observed in the transport activity of the UCP1 carrier, regulated by purine nucleotide binding sites on the matrix side [38]. Evidence of the existence of a specific binding site for ATP^{4-} also comes from the comparison of the binding free energy obtained in the X docking of ATP^{4-} and GTP^{4-}. The values are −8.13 and −2.52 kcal mol^{-1} for ATP^{4-} and GTP^{4-}, respectively, and correspond to a difference in their dissociation constants of the order of 10^4, indicating that the carrier displays a specific site for ATP^{4-}. The ATP^{4-} interaction site is formed from three positively charged amino acids (Lys48, Arg59, Lys146), two polar amino acids (Gln43, Gln150), one negatively charged amino acid (Glu63), and a glycine (Gly145). These amino acids determine the binding of the substrate in a unique orientation where the phosphate groups are stabilized by the positively charged residues (Lys48, Arg59, Lys146) (Table 1). The positive residues rigidly anchor the phosphate groups, while the base moiety can change its position because it can equally interact with two glutamines (Gln43 and Gln150) that are located one in front of the other (Table 1 and Fig. 5a).

This site (site I) was found also in the MD docking runs, with the same global characteristics and a few important differences. The amino acids composing it are the same as for the X docking, with the exception that Gln49 replaces Gln43. Some differences are also observed in the 3D arrangement. In detail, in the MD docking, Gln49 mainly interacts with the phosphates, while Gln150 retains its interactions with the purine ring. The other and more notable difference involves Glu63 (which interacts with the sugar), because it is not involved in the electrostatic network that is present in the crystal structure, where it forms an electrostatic triad with Arg59 and Lys146. Rearrangements of salt bridges have been suggested to be important in the transport mechanism [17, 39, 40], and this was proposed to be the triggering mechanism for substrate-induced conformational change [21, 22, 36]. Indeed, significant changes at the level of the matrix region have been assessed by MD simulations performed in the absence of CATR [19, 27]. As can be seen in the representative snapshot in Fig. 5b, Glu63 does not bridge the same positive residues as before, and is now able to make a bond with the sugar moiety. The different spreads in the positioning of the ATP^{4-} molecules in X and MD docking (Fig. 3c, d) are due to the RMSF values of the amino acids interacting with the ligand (Fig. 6). In site I, Glu63 and Gln150, which interact with the sugar and the base moiety, respectively, have RMSF values lower than those of Lys48, Arg59, and Lys146, which interact with the phosphate. It is

worth noting that, in spite of the rearrangements of the residues and the dispersion in the orientations of the substrate moieties, site I as found in the crystal structure was also maintained in the structures extracted from the MD simulation.

In MD docking, another interaction site—site II—appeared that was not mapped in X docking (Fig. 3d). The new site consisted of two positively charged amino acids (Lys432, Arg243), one polar amino acid (Gln240), one negatively charged amino acid (Asp247), and one hydrophobic amino acid (Met249). The physicochemical characteristics of site II were almost the same as those observed for site I, in fact the phosphate moiety of the substrate is stabilized by the positively charged amino acids, the basic moiety by the polar and hydrophobic residues, and the negatively charged amino acid stabilizes the sugar (Table 1). In site II, the positions of the phosphate groups are variable, and that of the base even more so, due to the large fluctuations of the amino acids that form the binding site (Fig. 5). This is shown by the bidirectional arrows in Fig. 3d, whose lengths are proportional to the spread of the clustered ligands on the surface.

The presence in MD docking of two interaction sites located in two distinct matrix areas may be related to the tripartite structure of the protein. Experimental studies have shown that the substrate transport is 1:1, so the carrier channel can only be crossed by one molecule at a time [39]. This is due to the carrier assembly, which does not permit more than one molecule to pass through the channel at the same time because of steric hindrance. Recent studies have highlighted the symmetric and asymmetric conservation of residues in the mitochondrial carrier family [36], and identified three symmetrical substrate contact points in the bottom of the channel and three toward the intermembrane space, each one located on a single repeat. In addition, even though it has long been thought that mitochondrial carriers function as dimers, the dimer interface is still elusive, and new data hint that a monomer is the functional unit [41], supporting the use of a monomeric model system.

The analyzed MD structures show the occurrence of two binding sites for the ATP^{4-} substrate, each one spreading in a region involving two repeats. The residues of site I are located on repeats 1 and 2, and those of site II are located on repeats 3 and 1 (Fig. 4). These residues are highly conserved in a large number of sequences taken from different species that are far apart evolutionarily (Fig. S4), suggesting the involvement of these residues in the formation of a conserved ATP^{4-} binding site. Extending the symmetry considerations for the tripartite sequence and the three-dimensional structure of the repeats, the existence of a third binding site could be expected.

Summary

The coupling of MD and protein–ligand docking allowed us to suggest the residues of the bovine mitochondrial ADP/ATP carrier that are involved in binding the ATP^{4-} substrate in the matrix region (Fig. 3). Applying molecular docking to the c-state X-ray structure of the transporter [17] led us to identify a unique binding site that, in the absence of CATR, is ready to preliminarily interact with ATP in the matrix region, which may trigger complex molecular machinery that is able to invert the transport process. This site was also detected by docking performed on the structures extracted from the MD simulation carried out on the free carrier, which also highlighted a second binding site that was arranged in a similar way to the first one, and contained amino acids with similar physical chemical properties to those in the first site (Table 1 and Fig. 5). These findings beg the question of whether the multiple sites act independently or via a concerted mechanism driven by the ATP^{4-} concentration in the matrix region.

Acknowledgments The authors would like to thank the CASPUR Interuniversity Consortium for the Application of Supercomputing for Universities and Research (Rome, Italy) for the use of the parallel computer MATRIX.

References

1. Palmieri F (2004) The mitochondrial transporter family (SLC25): physiological and pathological implications. Pflug Arch 447:689–709
2. Torroni A, Stepien G, Hodge JA, Wallace DC (1990) Neoplastic transformation is associated with coordinate induction of nuclear and cytoplasmic oxidative phosphorylation genes. J Biol Chem 265:20589–20593
3. Heddi A, Lestienne P, Wallace DC, Stepien G (1993) Mitochondrial DNA expression in mitochondrial myopathies and coordinated expression of nuclear genes involved in ATP production. J Biol Chem 268:12156–12163
4. Kaukonen J, Juselius JK, Tiranti V, Kyttälä A, Zeviani M, Comi GP, Keränen S, Peltonen L, Suomalainen A (2000) Role of adenine nucleotide translocator 1 in mtDNA maintenance. Science 289:782–785
5. Fiore C, Arlot-Guilligay D, Trézéguet V, Lauquin GJ, Brandolin G (2001) Fluorometric detection of ADP/ATP carrier deficiency in human muscle. Clin Chim Acta 311:125–135
6. Napoli L, Bordoni A, Zeviani M, Hadjigeorgiou GM, Sciacco M, Tiranti V, Terentiou A, Moggio M, Papadimitriou A, Scarlato G, Comi GP (2001) A novel missense adenine nucleotide translocator-1 gene mutation in a Greek adPEO family. Neurology 57:2295–2298
7. Ricquier D, Casteilla L, Bouillaud F (1991) Molecular studies of the uncoupling protein. FASEB J 5:2237–2242
8. Walker JE, Runswick MJJ (1993) The mitochondrial transport protein superfamily. Bioenerg Biomembr 25:435–446
9. Jezek P, Jezek J (2003) Sequence anatomy of mitochondrial anion carriers. FEBS Lett 534:15–25

10. Vignais PV (1976) Molecular and physiological aspects of adenine nucleotide transport in mitochondria. Biochim Biophys Acta 456:1–38
11. Klingenberg M (1989) Molecular aspects of the adenine nucleotide carrier from mitochondria. Arch Biochem Biophys 270:1–14
12. Vignais PV, Vignais PM, Stanislas E (1962) Action of potassium atractylate on oxidative phosphorylation in mitochondria and in submitochondrial particles. Biochim Biophys Acta 60:284–300
13. Henderson PJ, Lardy HAJ (1970) Bongkrekic acid. An inhibitor of the adenine nucleotide translocase of mitochondria. Biol Chem 245:1319–1326
14. Klingenberg M (2008) The ADP and ATP transport in mitochondria and its carrier. Biochim Biophys Acta 1778:1978–2021
15. Kunji ER, Harding M (2003) Projection structure of the atractyloside-inhibited mitochondrial ADP/ATP carrier of *Saccharomyces cerevisiae*. J Biol Chem 278:36985–36988
16. Dahout-Gonzalez C, Brandolin G, Pebay-Peyroula E (2003) Crystallization of the bovine ADP/ATP carrier is critically dependent upon the detergent-to-protein ratio. Acta Crystallogr D 59:2353–2355
17. Pebay-Peyroula E, Dahout-Gonzalez C, Kahn R, Trézéguet V, Lauquin GJM, Brandolin G (2003) Structure of mitochondrial ADP/ATP carrier in complex with carboxyatractyloside. Nature 426:39–44
18. Nury H, Dahout-Gonzalez C, Trézéguet V, Lauquin G, Brandolin G, Pebay-Peyroula E (2005) Structural basis for lipid-mediated interactions between mitochondrial ADP/ATP carrier monomers. FEBS Lett 579:6031–6036
19. Falconi M, Chillemi G, Di Marino D, D'Annessa I, Morozzo della Rocca B, Palmieri L, Desideri A (2006) Structural dynamics of the mitochondrial ADP/ATP carrier revealed by molecular dynamics simulation studies. Proteins 65:681–691
20. Rey M, Man P, Clemencon B, Trézéguet V, Brandolin G, Forest E, Pelosi L (2010) Conformational dynamics of the bovine mitochondrial ADP/ATP carrier isoform 1 revealed by hydrogen/deuterium exchange coupled to mass spectrometry. J Biol Chem 285:34981–34990
21. Wang Y, Tajkhorshid E (2008) Electrostatic funnelling of substrate in mitochondrial inner membrane carriers. Proc Natl Acad Sci USA 105:9598–9603
22. Dehez F, Pebay-Peyroula E, Chipot C (2008) Binding of ADP in the mitochondrial ADP/ATP carrier is driven by an electrostatic funnel. J Am Chem Soc 130:12725–12733
23. Krammer EM, Ravaud S, Dehez F, Frelet-Barrand A, Pebay-Peyroula E, Chipot C (2009) High-chloride concentrations abolish the binding of adenine nucleotides in the mitochondrial ADP/ATP carrier family. Biophys J 97:L25–L27
24. Feng J, Lucchinetti E, Enkavi G, Wang Y, Gehrig P, Roschitzki B, Schaub MC, Tajkhorshid E, Zaugg K, Zaugg M (2010) Tyrosine phosphorylation by Src within the cavity of the adenine nucleotide translocase 1 regulates ADP/ATP exchange in mitochondria. Am J Physiol Cell Physiol 298:C740–C748
25. Majima E, Shinohara Y, Yamaguchi N, Hong YM, Terada H (1994) Importance of loops of mitochondrial ADP/ATP carrier for its transport activity deduced from reactivities of its cysteine residues with the sulfhydryl reagent eosin-5-maleimide. Biochemistry 33:9530–9536
26. Majima E, Yamaguchi N, Chuman H, Shinohara Y, Ishida M, Goto S, Terada H (1998) Binding of the fluorescein derivative eosin Y to the mitochondrial ADP/ATP carrier: characterization of the adenine nucleotide binding site. Biochemistry 37:424–432
27. Di Marino D, Oteri F, Morozzo Della Rocca B, Chillemi G, Falconi M (2010) ADP/ATP mitochondrial carrier MD simulations to shed light on the structural–dynamical events that, after an additional mutation, restore the function in a pathological single mutant. J Struct Biol 172:225–232
28. Lindahl E, Hess B, van der Spoel D (2001) GROMACS 3.0: a package for molecular simulation and trajectory analysis. J Mol Model 7:306–317
29. Daura X, van Gunsteren WF, Mark AE (1999) Folding–unfolding thermodynamics of a beta-heptapeptide from equilibrium simulations. Proteins 34:269–280
30. Morris GM, Goodsell DS, Halliday RS, Huey R, Hart WE, Belew RK, Olson AJ (1998) Automated docking using a Lamarckian genetic algorithm and an empirical binding free energy function. J Comput Chem 19:1639–1662
31. Morris GM, Huey R, Lindstrom W, Sanner MF, Belew RK, Goodsell DS, Olson AJ (2009) AutoDock4 and AutoDockTools4: automated docking with selective receptor flexibility. J Comput Chem 30:2785–2791
32. Humphrey W, Dalke A, Schulten K (1996) VMD—visual molecular dynamics. J Mol Graph 14:33–38
33. Pettersen EF, Goddard TD, Huang CC, Couch GS, Greenblatt DM, Meng EC, Ferrin TE (2004) UCSF Chimera—a visualization system for exploratory research and analysis. J Comput Chem 25:1605–1612
34. Klingenberg M (2005) Ligand–protein interaction in biomembrane carriers: the induced transition fit of transport catalysis. Biochemistry 44:8563–8570
35. Robinson AJ, Kunji ER (2006) Mitochondrial carriers in the cytoplasmic stat have a common substrate binding site. Proc Natl Acad Sci USA 103:2617–2622
36. Robinson AJ, Overy C, Kunji ER (2008) The mechanism of transport by mitochondrial carriers based on analysis of symmetry. Proc Natl Acad Sci USA 105:17766–17771
37. Duyckaerts C, Sluse-Goffart CM, Fux J, Sluse FE, Liebecq C (1980) Kinetic mechanism of the exchanges catalysed by the adenine-nucleotide carrier. Eur J Biochem 106:1–6
38. Arechaga I, Ledesma A, Rial E (2001) The mitochondrial uncoupling protein UCP1: a gated pore. IUBMB Life 52:165–173
39. Nury H, Dahout-Gonzalez C, Trézéguet V, Lauquin GJ, Brandolin G, Pebay-Peyroula E (2006) Relations between structure and function of the mitochondrial ADP/ATP carrier. Annu Rev Biochem 75:4.1–4.29
40. Nelson DR, Felix CM, Swanson JM (1998) Highly conserved charge-pair networks in the mitochondrial carrier family. J Mol Biol 277:285–308
41. Kunji ER, Crichton PG (2010) Mitochondrial carriers function as monomers. Biochim Biophys Acta 1797:817–831